Electronic Supplementary Material (ESI) for Journal of Materials Chemistry A.
This journal is © The Royal Society of Chemistry 2017

Supplementary Information

An innovative carbon template-induced approach to graphene-like MnO_2 nanomesh with enhanced pseudocapacitance performance

Ziya Wang,[a] Fengping Wang*[a]

Department of Physics, School of Mathematics and Physics, University of Science and Technology Beijing, Beijing, PR China
Corresponding author: fpwang@ustb.edu.cn (F. Wang)

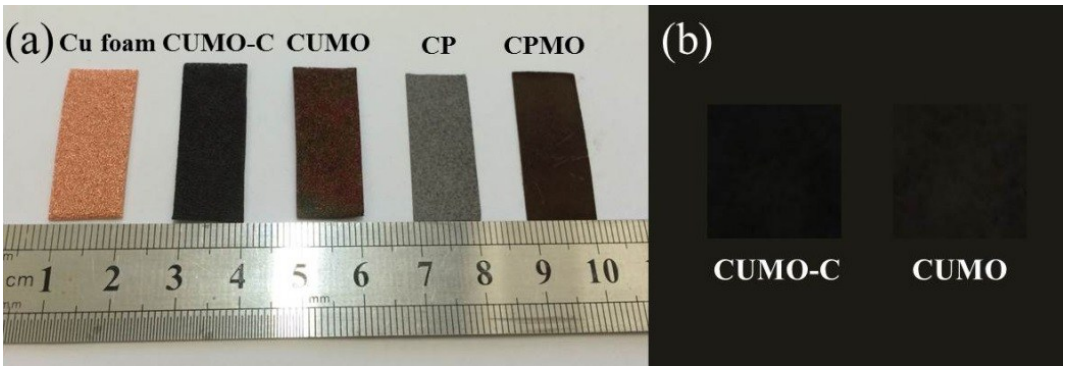

Fig. S1 (a) Photographs of Cu foam, CUMO-C, CUMO, CP and CPMO with size of 3×1 cm^2. (b) The color contract of the powder (peeled from the substrate) of CUMO-C (near black) and CUMO (brown), suggesting their different structures.

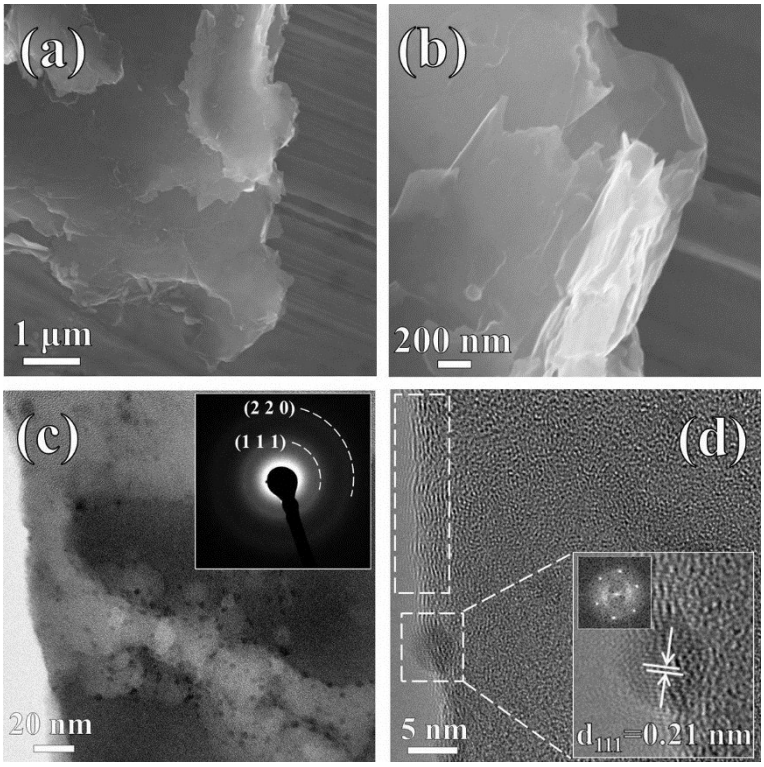

Fig. S2 (a-b) SEM and (c-d) TEM images of CUC under different magnifications. The inset of (c) is the corresponding SAED pattern. Two blurred diffraction rings agree with the (111) and (220) planes

of Cu phase, respectively. The inset in (d) is the HRTEM image of a Cu nanoparticle, reveals the small Cu particles with a lattice spacing of ~0.21 nm, corresponding to the (111) plane of the face-centered cubic Cu crystalline lattice.

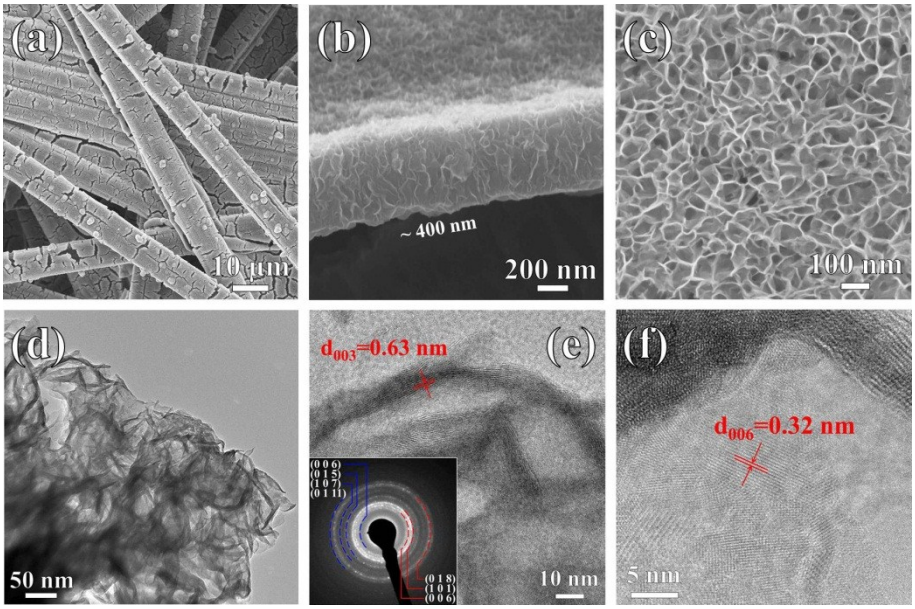

Fig. S3 (a) the low magnification, (b) cross-section and (c) top view SEM images of CPMO. (d-f) TEM images with different magnifications. The inset in (e) is the SAED pattern. (the red and blue signs stand for the $K_{0.47}Mn_{0.94}O_2$ phase and $K_{0.27}MnO_2{\cdot}(H_2O)_{0.54}$ phase, respectively.)

SEM images of CPMO at different magnifications are presented in Figure S3(a-c). Obviously, the film exhibits a representative K-birnessite MnO_2 characteristics, as many earlier reports.[1] These interconnected nanoflakes grow vertically and closely on the surface of carbon paper, forming a mesoporous film with ~400 nm thickness. On the other hand, TEM images give the obvious differences with that of CUMO-C, including nanoflakes with bigger sizes and better crystallinity and a two-phase construction. Although the resolved lattice fringes of 0.63 nm and 0.32 nm correspond to the (003) and (006) planes of $K_{0.47}Mn_{0.94}O_2$, respectively. The complex diffraction patterns confirm the existence of affiliated $K_{0.27}MnO_2{\cdot}(H_2O)_{0.54}$ phase.

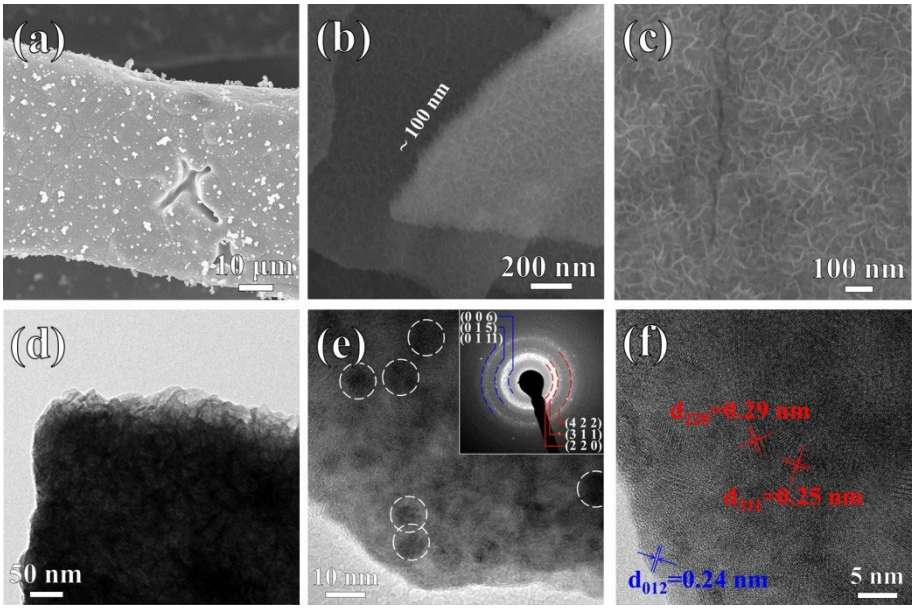

Fig. S4 (a-c) SEM images of CUMO with different magnifications. (d-f) TEM images of CUMO under different magnifications. Inset of (e) is corresponding SAED pattern. (the red and blue signs stand for the $CuMn_2O_4$ phase and $K_{0.27}MnO_2{\cdot}(H_2O)_{0.54}$ phase, respectively.)

The morphology and microstructure of the as-prepared CUMO nanostructures were analyzed by microscopy. It is obvious that the thin layer of CUMO film (~100 nm) was self-assembled by the interlaced nanoflakes, as shown in SEM images. While through the TEM analysis, the discernible $CuMn_2O_4$ nanoparticles as a result of reaction between Cu nanoparticles of Cu foam surface and $KMnO_4$ were embedded in the MnO_2 matrix. The accurate phase distribution of CUMO was further verified by TEM observation of Figure S4(d-f). The selected lattice fringes from the nanoparticles and edge regions, manifestly correspond to the (220) and (311) planes of cubic $CuMn_2O_4$ and the (012) planes of $K_{0.27}MnO_2{\cdot}(H_2O)_{0.54}$, respectively. Combined with the unambiguous SAED patterns, it can demonstrate the polycrystalline and near bulk nature of K-birnessite MnO_2 nanoflakes for CUMO. In short, Cu foam provide a suitable condition to generate such interesting $MnO_2/CuMn_2O_4$ nanocomposites.

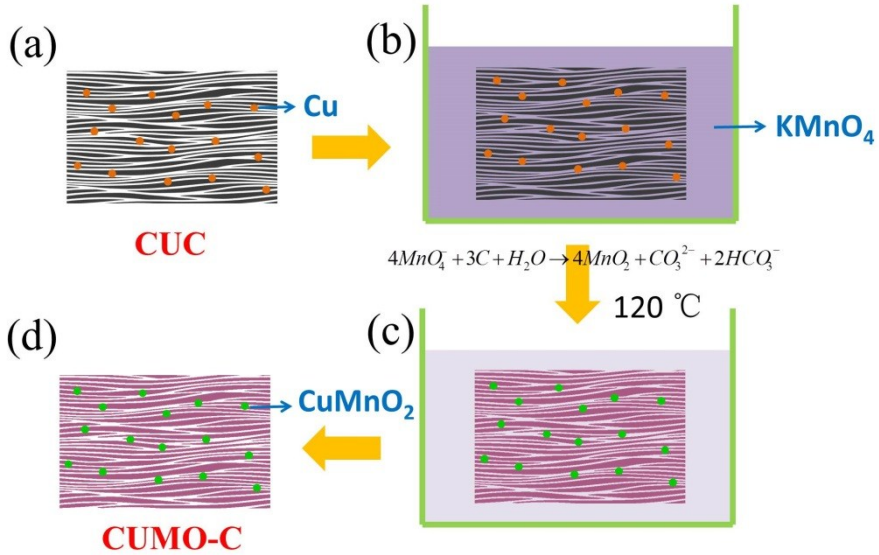

Fig. S5 The fabrication process of CUMO-C. (a) the laminar carbon template with dispersed Cu nanoparticles. (b-c) In the $KMnO_4$ solution of hydrothermal condition, MnO_4^- can insert into the interlayer and defects of CUC and in situ react with layered amorphous carbon. (d) Finally, the scarified template are exhausted and living the graphene-like MnO_2 nanomesh with intercalated $CuMnO_2$ nanoparticles (CUMO-C).

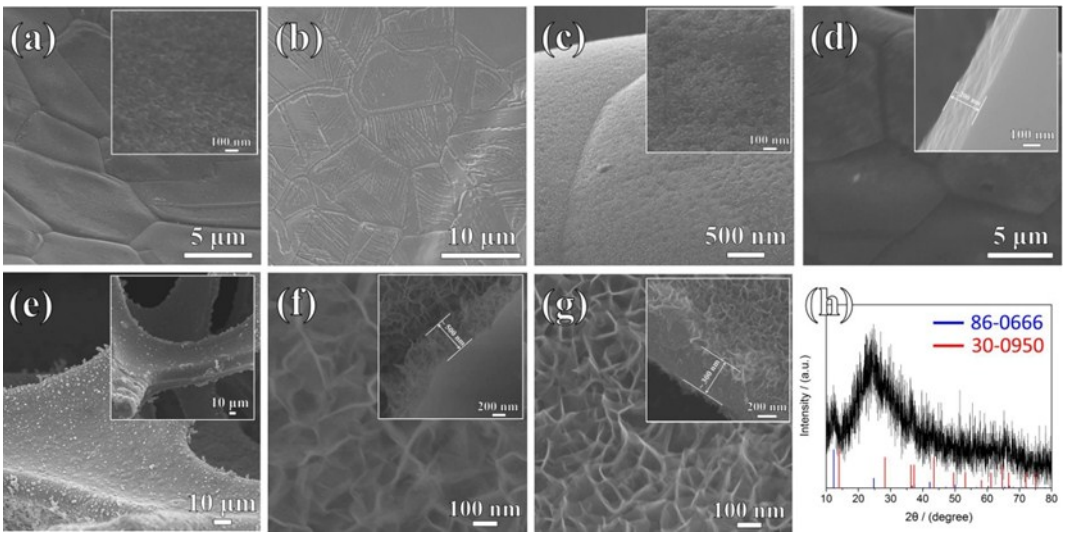

Fig. S6 The other metal—Ni (Ni foam) was used to repeat the growth process of CUMO-C for prove the necessity of metal Cu. (a) SEM image of Ni foam surface, inset is the magnified fine structure. Compared with Cu foam, just few oxides are found on the surface of Ni foam (O (wt%):0.84 (Cu) vs. 14.10 (Ni)). (b) Nickel foam surface after direct carbonization treatment. Here different from CUC,

small amount of carbon products can be attached to the surface of Ni due to lack of sufficient chemical reaction between glucose and surface oxides. (c) the artificial Ni oxides after a 400 ℃ calcination and (d) followed carbonized products (NIC). Insets are corresponding magnified images. The thickness of NIC is about 200 nm and has the layered features. (e) SEM image of NIMO-C which was prepared by same steps as CUMO-C, only replacing the CUC with NIC. Inset of (e) is the SEM image of NIMO directly used Ni foam as substrate. (f) and (g) are the high magnification of NIMO and NIMO-C, respectively. It is compared that NIMO and NIMO-C present the semblable morphology. (h) The XRD pattern of NIMO-C powders. Similar to CUMO-C, the $K_{0.47}Mn_{0.94}O_2$ (JCPDS 30-0950) is the main phase of NIMO-C, but crucially the (003) peak which represents the interlaminar spacing is still remains.

Through above basic measurements, we can conclude that, first, the metal oxides which is essential to stickness of glucose and formed laminar amorphous carbon product. Second, Ni although plays a positive role in mono/few layered MnO_2 nanosheets, Cu nanoparticles as a better catalyst achieves a perfect graphene-like MnO_2 nanomesh.

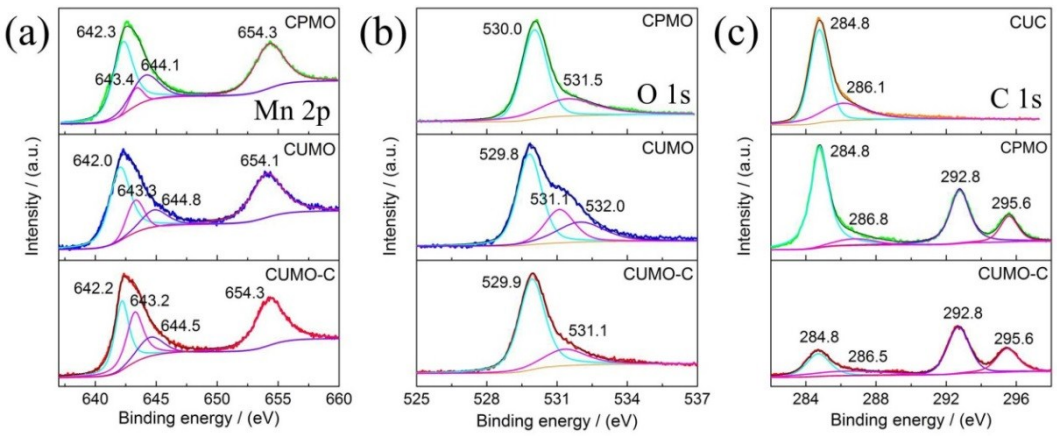

Fig. S7 Deconvoluted (a) Mn 2p and (b) O 1s XPS spectra of the CPMO, CUMO and CUMO-C, respectively. (c) Deconvoluted C 1s XPS spectra of the CUC, CPMO and CUMO-C.

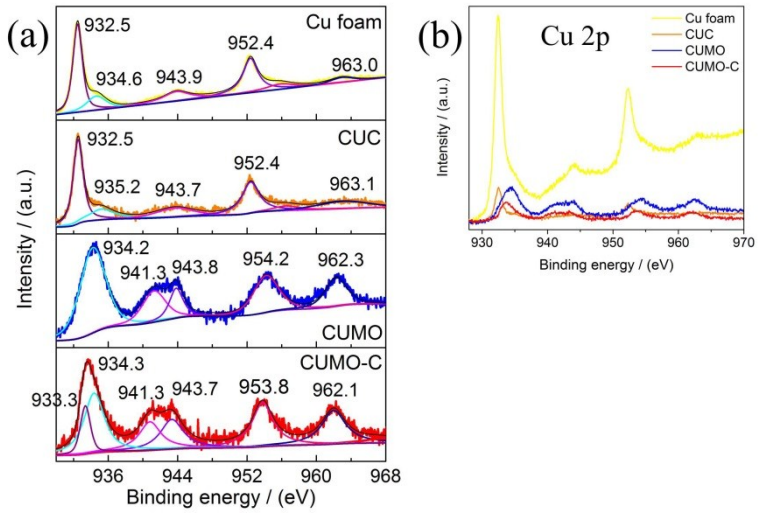

Fig. S8 (a) Deconvoluted Cu 2p XPS spectra of the Cu foam, CUC, CUMO and CUMO-C, and (b) their intensity contrast.

Figure S7 main illustrates the oxidation states of Cu of involved samples, which determines the composition of scattered nanoparticles. The Cu 2p spectra of Cu foam and CUC show the similar characteristics but very different intensity. The Cu 2p 3/2 peak are resolved two components, which can be assigned to Cu^0 (932.5 eV) and Cu^{2+} (934.6 eV),[2] indicating that the nanoparticles in CUC is Cu particles with slight oxide content (CuO), as same as our TEM conclusions. In contrast, the Cu 2p 3/2 peak of CUMO exhibits only one peak located at 934.2 eV along with two satellite peaks at 941.3 and 943.8 eV, demonstrating the transformation of $CuMn_2O_4$ from Cu nanoparticles. Furthermore, the additional peaks of CUMO-C at 933.3 eV can be attribute to the Cu^+,[3] also proves the existence of $CuMnO_2$. Namely parts of Cu nanoparticles have not been oxidized to $CuMn_2O_4$, but become the Cu^+ with the involvement of amorphous carbon.

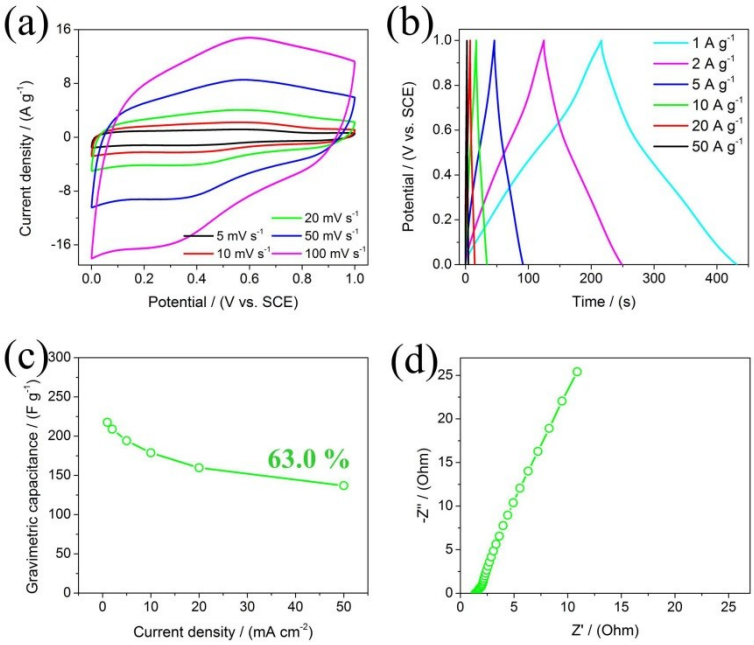

Fig. S9 (a) CV curves, (b) GCD curves, (c) rate capability and (d) EIS of CPMO by the direct measurement. Obviously, due to these MnO_2 nanoflakes grow directly on conductive substrates (carbon paper), which is regarded as beneficial to improving the conductive connection between the active material and current collector, reducing the "dead volume" and resistance possibly caused by the polymer binder, the "CPMO" get the bigger size of CV curve area, the longer charge/discharge time, the higher rate capability and lower resistance of equivalent electric circuit. The calculated specific capacitance is about 217.5 F g^{-1} at a current density of 1 A g^{-1}.

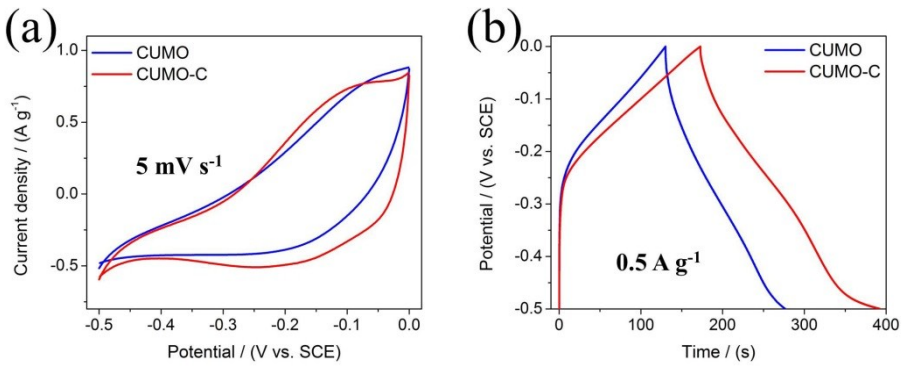

Fig. S10 (a) CV and (b) GCD curves of CUMO and CUMO-C directly measured at 5 mV s^{-1} and 0.5 A g^{-1}, respectively. Note that our potential window is unusual -0.5-0 V for avoiding the electrochemical reaction of Cu substrate. The CUMO-C with high loading mass (4.25 mg cm^{-2}) still exhibits the

advantages on the pseudocapacity (172.8 F g^{-1} vs. 130.1 F g^{-1} at 0.5 A g^{-1})compared with CUMO of low loading mass (1.48 mg cm^{-2}).

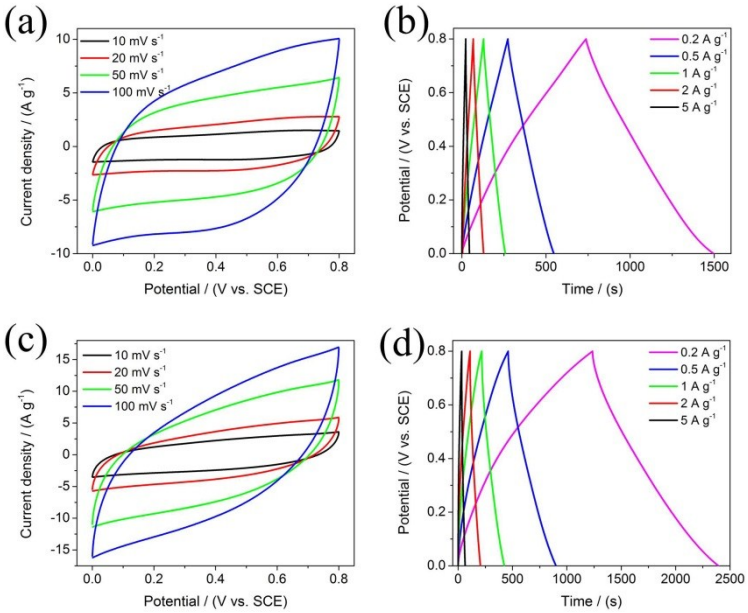

Fig. S11 (a) CV and (b) GCD curves of CPMO at various rates. (c) CV and (d) GCD curves of CUMO at different scan rates and current densities, respectively.

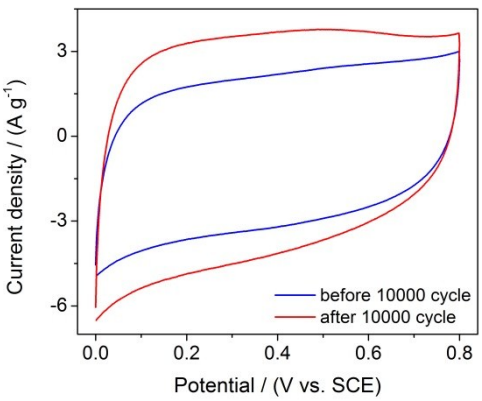

Fig. S12 The cyclic voltammetry curves of CUMO-C collected before and after 10000 cycles,

demonstrating improved pseudocapacitance as the cycle numbers increase.

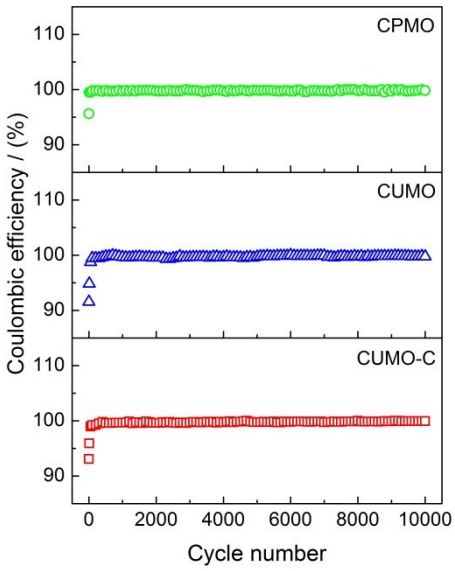

Fig. S13 Coulombic efficiency of CPMO, CUMO and CUMO-C at a current rate of 10 A g^{-1}. The near 100 % coulombic efficiency indicates outstanding long-term electrochemical stability and reversibility of the three samples.

References

1 S. Devaraj and N. Munichandraiah, *J. Phys. Chem. C*, 2008, **112**, 4406-4417.

2 X. Xu, M. Han, J. Ma, C. Zhang and G. Li, *RSC Adv.*, 2015, **5**, 71760-71764.

3 J. Gong, H. Yue, Y. Zhao, S. Zhao, L. Zhao, J. Lv, S. Wang and X. Ma, *J. Am. Chem. Soc.*, 2012, **134**, 13922-13925.